Study on the Influence of the Magnetic Field Topology on the Power Deposition in a Helicon Plasma Source

M. Magarotto, M. Manente, P. de Carlo, F. Trezzolani, D. Pavarin, and D. Melazzi
CISAS, Padova, Italy

Abstract: We have numerically studied how actual confinement magneto-static field lines affect power deposition in a Helicon source. We have solved the wave propagation by means of SPIREs, a 1D-radial finite-difference frequency-domain electromagnetic solver. We have calculated the radial power deposition profile for different radial gradient profiles of the magneto-static field B_0. We have analyzed two configurations of magneto-static field: Maxwell, and Helmholtz coils. For each coils configuration we have studied three cases: i) low-density $n = 10^{17}$ m^{-3} and low-magnetic-field $B_0 = 250$ G; ii) medium-density $n = 10^{18}$ m^{-3} and medium-magnetic-field $B_0 = 500$ G; iii) high-density $n = 10^{19}$ m^{-3} and high-magnetic-field $B_0 = 1000$ G. If the magneto-static field is purely axial the power deposition profiles are peaked near the outer radius of the plasma source, and profiles associated to axial wave numbers k_z of opposite sign are perfectly superposed. In the Maxwell coil configuration power deposition profiles are peaked near the outer radius of the plasma source, but profiles associated to k_z of opposite sign are no more perfectly superposed; while the Helmholtz coil configuration leads to a power deposition profile peaked near the axis of the discharge.

I. Introduction

Plasma-based propulsion systems are beginning to challenge the monopole of chemical thrusters in space applications. The high specific impulse (which allows for a huge reduction in the propellant mass) and high thrust efficiency make the plasma thruster an attractive solution for space propulsion. At the state of the art plasma propulsion devices, such as the ion engine and the Hall effect thruster, have proven to have good performances but exhibit some critical issues: i) their lifetimes are limited by the erosion of the extracting grids and the ceramic walls; ii) they need an external cathode for charge compensation. Recent advances in

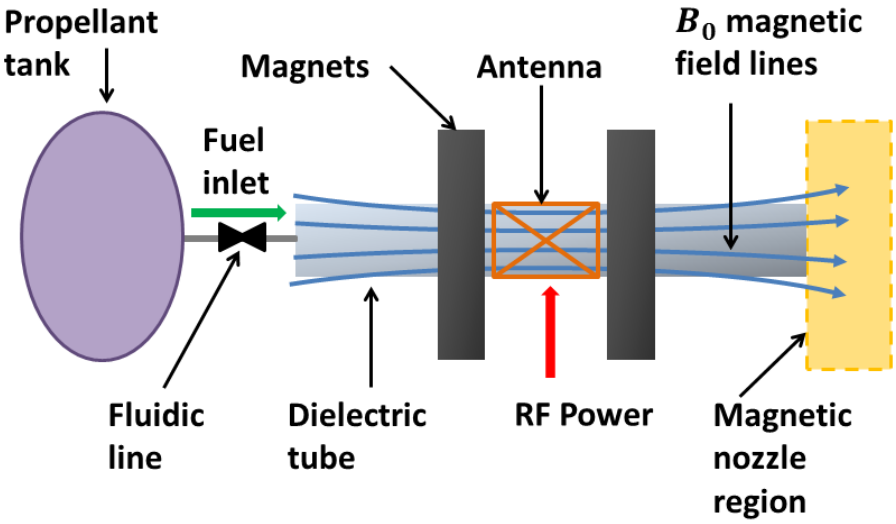

Figure 1. Helicon Plasma Thruster scheme.

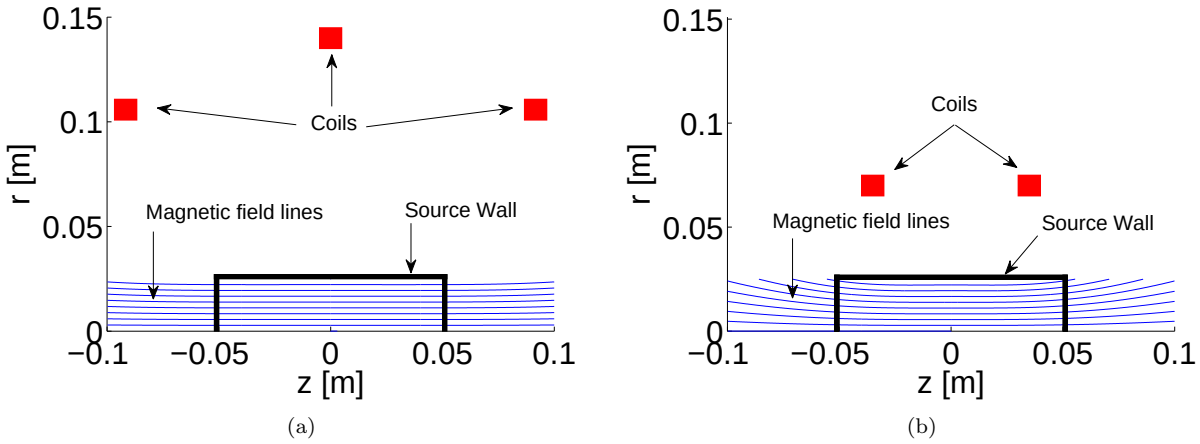

Figure 2. Draft of the magnetic field topology generated by: a) Maxwell's coils, b) Helholtz's coils.

plasma-based propulsion systems have led to the development of Helicon Plasma Thrusters[1] (HPTs), whose plasma-generation system is derived from high-density Helicon plasma sources.[2] HPTs are characterized by a long life (electrodes or neutralizers are not necessary in these thrusters), high specific impulses and good thrust efficiency.

In HPTs (see Figure 1) we can distinguish between the production stage (i.e. the Helicon source) and the acceleration stage, in which a magnetic nozzle is employed to accelerate the magnetized plasma. The production stage is composed of a gas feeding system (i.e. propellant tank and fluidic line), a Radio Frequency (RF) antenna, and magnets. The neutral gas is injected into a dielectric cylinder and ionized through a RF antenna working in the MHz regime; the magnets provide the magneto-static field that improves the confinement of the plasma and allows for the propagation of whistler waves.[3] The acceleration stage is realized by means of the divergent magnetic field lines at the exhaust section which provide a magnetic nozzle effect. HPTs are under study and development in some international research projects: the American VASIMR,[4] where a high-power Helicon source is coupled to a ion cyclotron resonance heating section to increase the specific impulse; the Europeans HPH.COM[5] in which a low-power ($\leq$100 W) system has been developed, and SAPERE-STRONG[6] that aims at the realization of a high-power ($\geq$1 kW) propulsive system to be employed in a space tug.

In HPTs the propulsive figures of merit depend on the plasma parameters (e.g. plasma density and electron temperature) inside the Helicon source. Plasma generation is mainly driven by the power deposited by the RF antenna into the source and the plasma transport therein. Therefore we need theoretical and numerical models of the wave propagation, and ultimately of the power deposition, to perform the design, and the optimization of HPTs. Many works tackle the power deposition by assuming confinement magneto-static field purely axial and uniform; however, actual Helicon sources applied in experimental setups for HPTs can depart from this assumption due to dimension, mass and power budget limitations.

Many works on Helicon sources have studied the physics of wave propagation and of power deposition. Main findings for uniform plasma sources are: i) two coupled Whistler waves, namely the Helicon and Trivelpiece-Gould waves,[3,7] propagate within the source; ii) the power deposition occurs mainly at the edge of the plasma cylinder, where the Trivelpiece-Gould waves are damped by collisional processes.[8] The influence of plasma non-uniformity has been widely investigated from both theoretical[9,10] and numerical[11,12] works. Less effort has been paid in studying the influence of non-uniform magneto-static fields on the wave propagation. A series of experimental works have been carried out in order to understand the enhancement of power deposited when the Helicon source is operating in non-uniform magnetic field. However, in all these works, the data interpretation has been based on simplified wave propagation models: Braginskij *et al.*,[13] used a dispersion relation that accounts for homogeneous magnetic field; Virko *et al.*,[14] employed a wave model that deal with an homogeneous magnetic field with non-null radial components; Guo *et al.*,[15] performed a comparative numerical analysis which accounts for non-homogeneities of the axial component of the confinement magnetic field. A detailed experimental campaign has been carried out by Lafleur *et al.*, in order to analyze the performances of a Piglet[16,17] Helicon reactor operating in non-uniform magnetic

field. In [16], the authors claimed that the axial distance over which waves propagate can be controlled through magnetic field strength and topology, the latter being critical in the region near the exit of the source; the results have been interpreted by relying on the Helicon dispersion relation derived in presence of uniform magnetic field. An experimental and numerical work on the Helicon waves propagation in non-uniform magnetic field has been carried out by Chang[18] *et al.*; they found that the Helicon wave has weaker attenuation away from the antenna in a focused magnetic field than in a uniform field. In the numerical tool employed in [18] radial component of magnetic field has been assumed with an axial expansion. Helicon sources working in non-uniform fields have been studied also in purely numerical works.[19,20] However, both in [19] and [20], the authors analyzed only one magnetic field topology: this prevent any insight on the influence of magnetic field components in the source performances, and ultimately on the power deposition.

We are interested in studying the effect of actual confinement magneto-static field on the power deposition phenomenon in Helicon plasma sources. In particular we have focused our attention on how gradients and radial components of magneto-static field distort the power deposition profile in respect to the ideal case of purely axial magnetic field. We have considered two magnetic field configurations, generated respectively by Maxwell's coils, and Helmholtz's coils (see Figure 2). The former provides an almost axial and uniform magneto-static field, while the latter introduces non-negligible gradients along radial and axial directions. We have resorted on the numerical tool SPIREs[21] to solve the wave propagation and in turn the power deposition. SPIREs is a 1D-radial finite-difference frequency-domain electromagnetic solver.

The paper is structured as follow: in section II, we will describe the numerical approach adopted; in section III, we will present the results obtained with magneto-static field generated by Maxwell's and Helmholtz's coils; in section IV, we will comment on the results.

II. Methodology

The Helicon source is assumed to be surrounded by a generic distribution of coaxial coils that generate the actual confinement magnetic field B_0. This very confinement field is axisymmetric with radial (B_{0r}) and axial (B_{0z}) components that depends on the radial (r) and axial (z) position within the source. Since we want to focus our attention on the influence of B_0 topology on the power deposition, we have assumed uniform plasma density n, electron temperature T_e, and neutral pressure p_0. Besides we relied on SPIREs, a 1D-radial finite-difference frequency-domain electromagnetic solver, to evaluate the Electro-Magnetic (EM) fields and, in turn, the power deposition profile.

We have assumed an harmonic dependence to time and space in the form of $\exp i(m\theta + k_z z - \omega t)$ for both fields and sources. In particular: i) m (i.e. the azimuthal wave number) is known from antenna geometry,[11] ii) ω depends on the antenna feeding system, iii) k_z (i.e. the axial mode number) depends on the plasma parameters (e.g. plasma density and electron temperature) and magneto-static field topology. To evaluate the propagative k_z we have resorted on the general dispersion relation that reads

$$K k_r^4 + \Lambda k_r^3 + M k_r^2 + N k_r + \Pi = 0 \tag{1}$$

where k_r is the propagative wave number in the radial direction, whereas the coefficients K, Λ, M, N, Π depend on k_z, m, B_{0r}, B_{0z}, and plasma parameters. The expression of the coefficients in Eq. 1 can be found in Cardinali, *et al.*[23] In particular the dispersion relation reported in Eq. 1 is employed as follow: we impose m, B_{0r}, B_{0z}, and we solve the dispersion relation for an interval of k_z, if the calculated k_r is real than the wave is propagative, otherwise not.

We have implemented in SPIREs an expression of the Stix tensor[22] (Eq. 2) that takes into account the general magneto-static field topology:

$$\boldsymbol{\varepsilon} = \begin{bmatrix} K_1 & K_4 & K_5 \\ -K_4 & K_2 & K_6 \\ K_5 & -K_6 & K_3 \end{bmatrix} \tag{2}$$

the definition of complex coefficients $K_n (n = 1 \dots 6)$ can be found in Swanson.[24]

Once we know the propagative m, k_z couples (calculated with the dispersion relation), we run SPIREs for each m, k_z propagative couple and we obtain the radial profiles of electric field $\mathbf{E}$, and dielectric current $\mathbf{J_p}$ spectra. Therefore we calculate the radial profile of the deposited power spectrum $P_r = 1/2 \int \int \mathbf{E} \cdot \mathbf{J_p} dz d\theta$.

III. Results

We have studied the power deposition in a Helicon source of radius $R = 0.025$ m, length $L = 0.10$ m, driven by a single loop antenna (i.e. azimuthal wave number $m = 0$) excited at a frequency $f = 13.56$ MHz, current flowing in the antenna $I = 1$ A. We have analyzed the magneto-static field B_0 generated by two coils configurations, namely Maxwell coils and Helmholtz coils (see Figure 2). Provided that we solve the EM fields with SPIREs, we can consider only radial profiles of B_0; therefore, in order to evaluate the effect of different B_0 gradients, we have analyzed for each coils configuration the B_0 profiles in correspondence of two axial sections, namely the center of the discharge $z = 0$ m, and the boundary of the discharge $z = 0.05$ m. The average value of B_{0z}, at the central axial section, has been studied in the range 250–1000 G. We have analyzed plasma density n from 10^{17} m^{-3} up to 10^{19} m^{-3}, pressure of neutral background $p_0 = 15$ mTorr, and electron temperature $T_e = 3$ eV. We will present the results obtained studying respectively the Maxwell and the Helmholtz coil configuration in three selected cases: i) low-density $n = 10^{17}$ m^{-3} and low-magnetic-field $B_0 = 250$ G, hereinafter referred to as *Case Low*; ii) medium-density $n = 10^{18}$ m^{-3} and medium-magnetic-field $B_0 = 500$ G, referred to as *Case Medium*; iii) high-density $n = 10^{19}$ m^{-3} and high-magnetic-field $B_0 = 1000$ G, referred to as *Case High*.

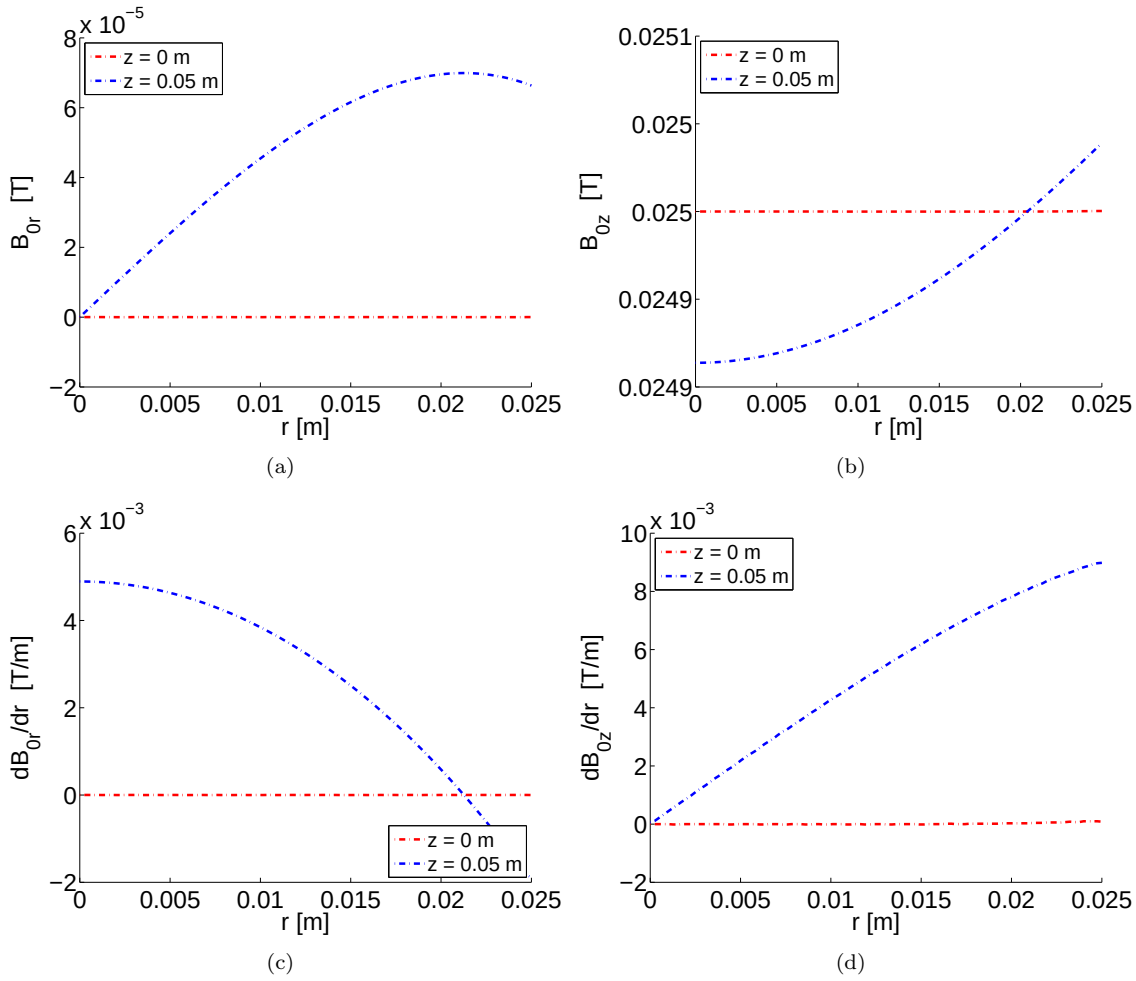

Figure 3. Maxwell's coil configuration in the low-magnetic-field case: confinement magnetic field B_0 along the radial direction r at two axial sections, namely z = 0 m (center of the discharge), z = 0.05 m (boundary of the discharge). a) B_0 radial component (B_{0r}), b) B_0 axial component (B_{0z}), c) gradient of B_{0r} along the radial direction, d) gradient of B_{0z} along the radial direction.

A. Maxwell Coils

In Figure 3 we have reported B_{0r}, B_{0z}, and their derivative along radial direction r for two axial sections, namely the center of the source ($z = 0$ m) and the boundary ($z = 0.05$ m). We have depicted only the low-magnetic-field case because the other cases can be derived by means of linearity. In the Maxwell coil configuration B_0 can be considered almost purely axial in the overall source.

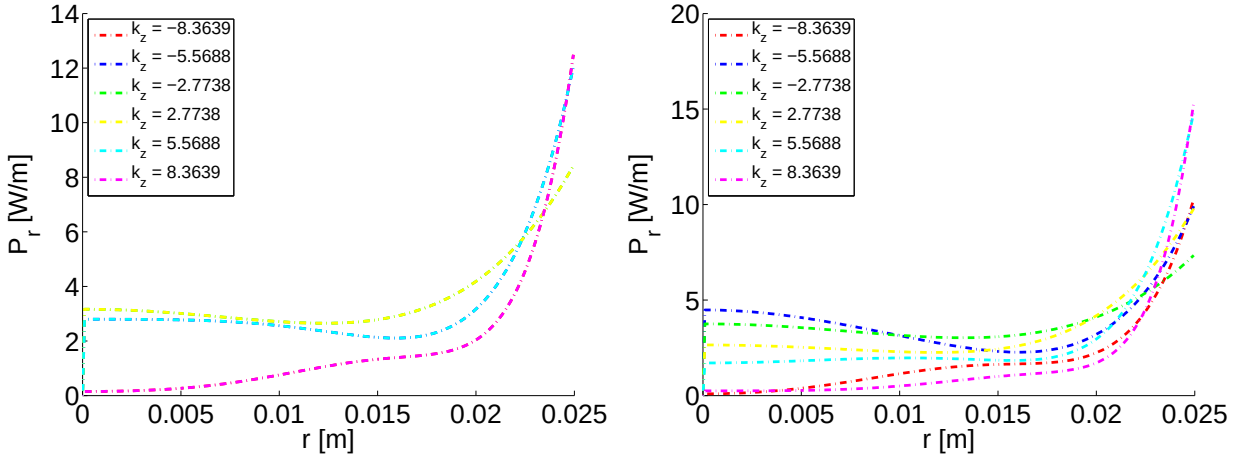

Figure 4. Maxwell's coil configuration; *Case Low* $\mathbf{n = 10^{17}\ m^{-3}}$, $\mathbf{B_0 = 250}$ G. Power deposition spectrum along the radial direction ($\mathbf{P_r}$) evaluated for different axial wave numbers $\mathbf{k_z}$. a) Center of the discharge $\mathbf{z = 0}$ m; b) boundary of the discharge $\mathbf{z = 0.05}$ m.

In Figure 4 the power deposition spectrum along the radial direction P_r is presented for the *Case Low* at $z = 0$ m, and $z = 0.05$ m. At $z = 0$ m (see Figure 4a), the power spectrum profiles for opposite values of k_z are perfectly superposed, while this does not hold true as soon as a B_{0r} component is introduced at $z = 0.05$ m (see Figure 4b). Nevertheless the B_0 non-homogeneities are not strong enough to modify the trend of the power spectrum profile: peaked near the outer radius of the plasma discharge.

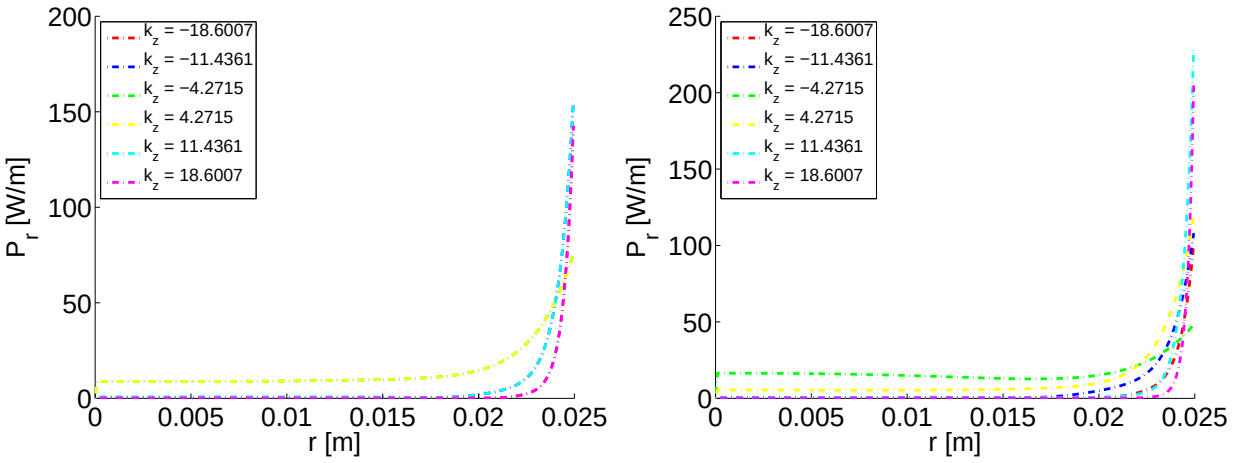

Figure 5. Maxwell's coil configuration; *Case Medium* $\mathbf{n = 10^{18}\ m^{-3}}$, $\mathbf{B_0 = 500}$ G. Power deposition spectrum along the radial direction ($\mathbf{P_r}$) evaluated for different axial wave numbers $\mathbf{k_z}$. a) Center of the discharge $\mathbf{z = 0}$ m; b) boundary of the discharge $\mathbf{z = 0.05}$ m.

In Figure 5, we have reported P_r for the *Case Medium* at $z = 0$ m, and $z = 0.05$ m. The power spectrum profiles at different axial sections present the same features of the *Case Low*. The main difference in respect to the *Case Low* is related to the height of the power deposition peak, in the *Case Medium* roughly one order of magnitude greater than in the *Case Low*.

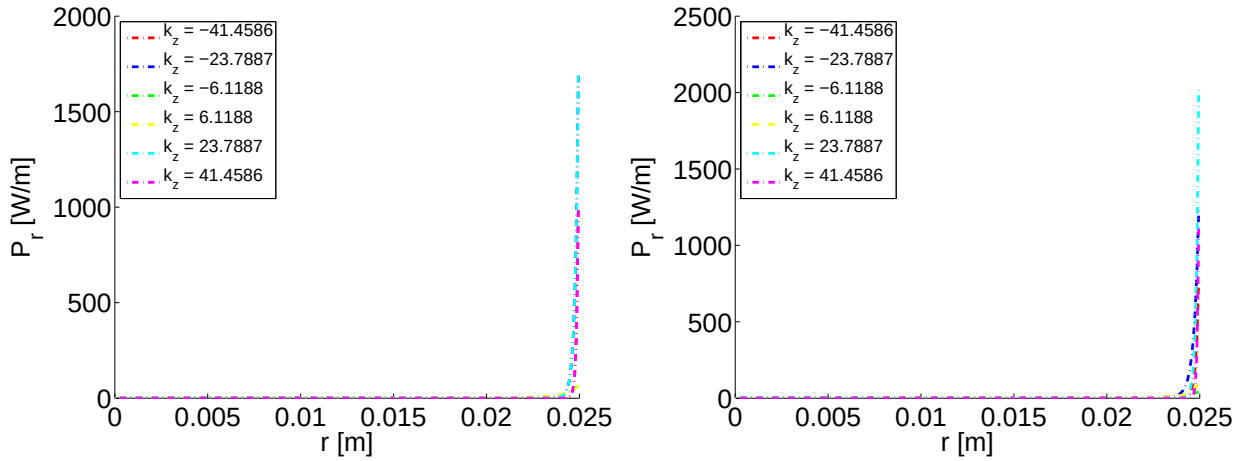

(a) (b)

Figure 6. Maxwell's coil configuration; *Case High* $\mathbf{n = 10^{19}\ m^{-3}}$, $\mathbf{B_0 = 1000}$ G. Power deposition spectrum along the radial direction ($\mathbf{P_r}$) evaluated for different axial wave numbers $\mathbf{k_z}$. a) Center of the discharge $\mathbf{z = 0}$ m; b) boundary of the discharge $\mathbf{z = 0.05}$ m.

In Figure 6, we have depicted P_r in the *Case High* at $z = 0$ m, and $z = 0.05$ m. The power spectrum profiles at different axial sections present the same features of the previous cases, but the height of the power deposition peak is roughly one order of magnitude greater than the *Case Medium*, and two orders of magnitude greater than the *Case Low*.

B. Helmholtz Coils

In Figure 7 we have reported B_{0r}, B_{0z}, and their derivative along radial direction r for two axial sections, namely the center of the source ($z = 0$ m) and the boundary ($z = 0.05$ m). We have depicted only the low-magnetic-field case because the other cases can be derived by means of linearity. In the Helmholtz coil configuration, at the source boundary B_0 is non-uniform and presents a non-negligible radial component.

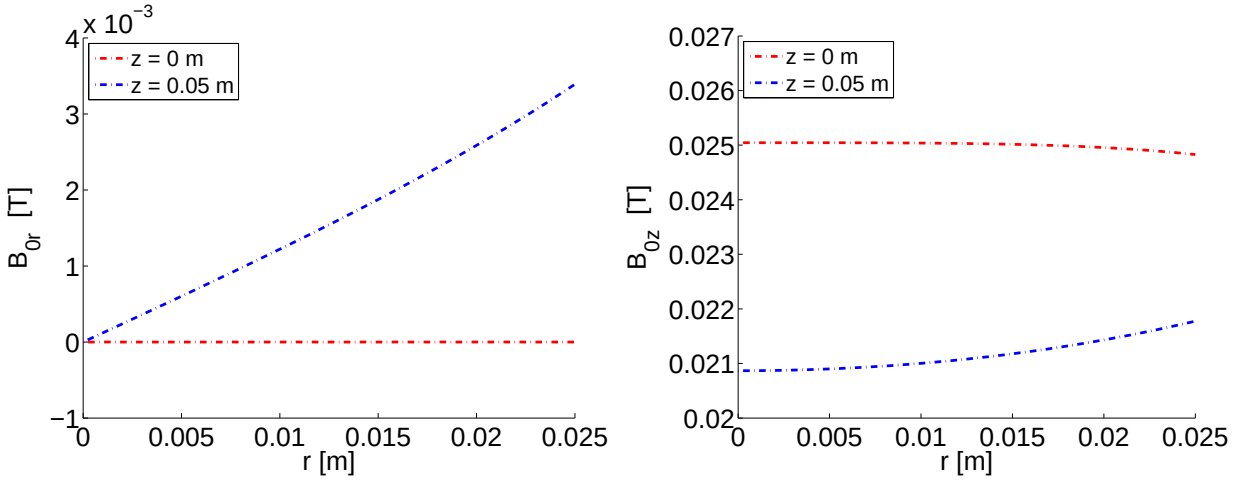

(a) (b)

In the *Case Low*, at $z = 0.05$ m (see Figure 8b) P_r is so much deformed that power deposition peak is near the axis of the source: this is in complete disagreement with results for B_0 almost uniform and axial (see Figure 8a). The deformed power deposition profile arises due to the radial components of B_0; in particular we want to point out that a ratio B_{0r}/B_{0z} in the order of 10% at the boundary of the source can produce a so intense distortion.

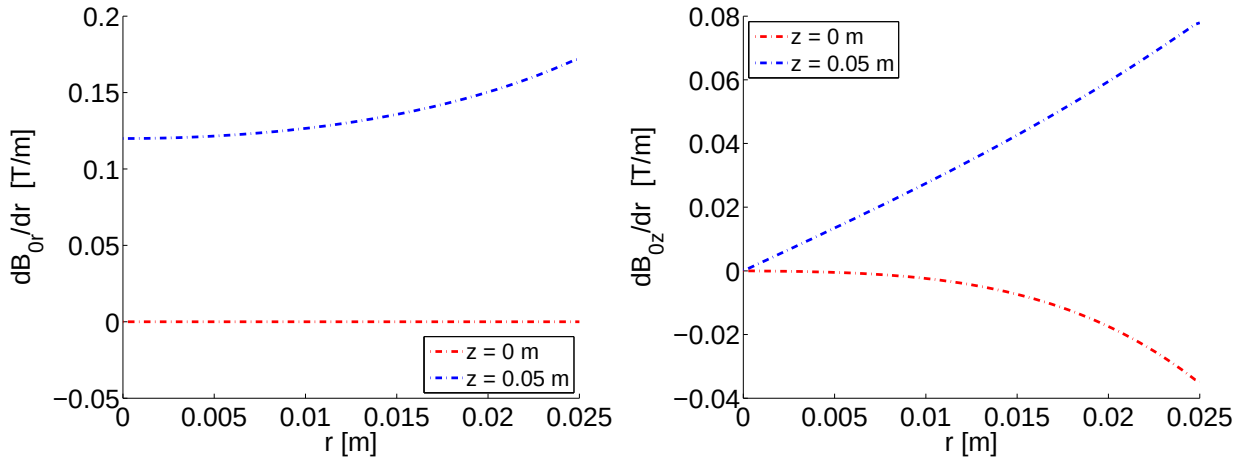

(c) (d)

Figure 7. Helmholtz's coil configuration in the low-magnetic-field case: confinement magnetic field B_0 along the radial direction r at two axial sections, namely z = 0 m (center of the discharge), z = 0.05 m (boundary of the discharge). a) B_0 radial component (B_{0r}), b) B_0 axial component (B_{0z}), c) gradient of B_{0r} along the radial direction, d) gradient of B_{0z} along the radial direction.

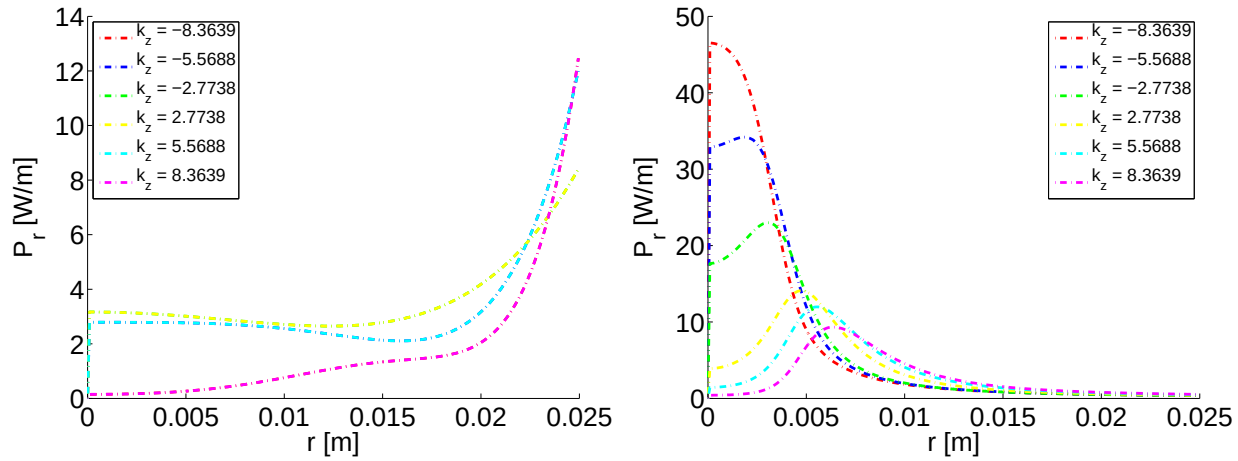

(a) (b)

Figure 8. Helmholtz's coil configuration *Case Low*: power deposition spectrum along the radial direction (P_r) evaluated for different axial wave numbers k_z. a) Center of the discharge z = 0 m; b) boundary of the discharge z = 0.05 m.

Also in the *Case Medium*, at the source boundary, the power deposition peak is near the axis of the source; on the contrary at the center of the discharge the power deposition peak is near the outer radius (see Figure 9). As it happens for the Maxwell's coil configuration, the power deposition profile has a peak one order of magnitude greater in the *Case Medium* in respect to the *Case Low*; this can be notice whether the power deposition profile is deformed or not.

In the *Case High*, as in the *Case Low* and in the *Case Medium*, at the source boundary, the power deposition peak is near the axis of the source; on the contrary at the center of the discharge the power deposition peak is near the outer radius (see Figure 10). Also with Helmholtz coils the power peak is one order of magnitude greater in *Case High* than in *Case Medium*, and two than in *Case Low*.

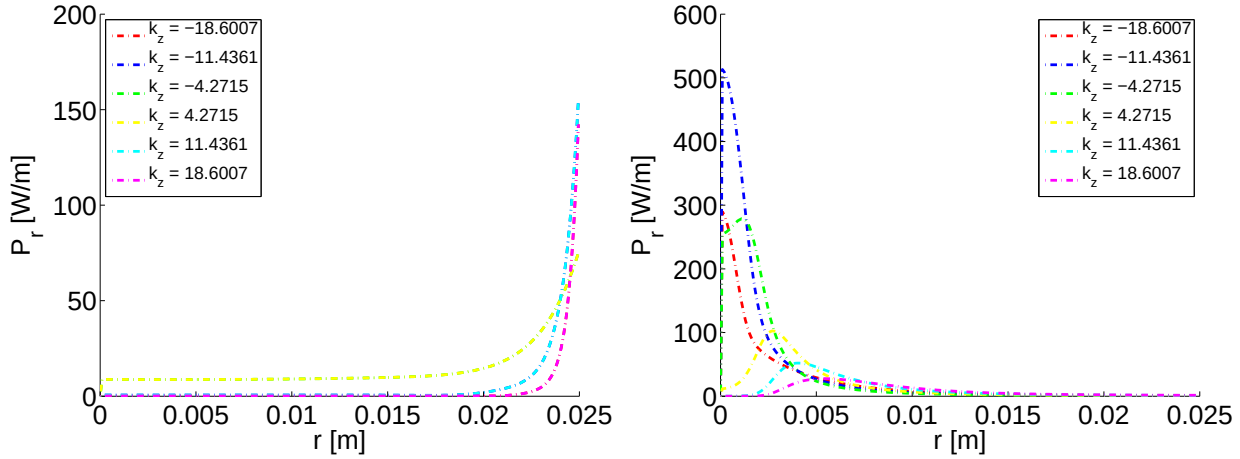

Figure 9. Helmholtz's coil configuration *Case Medium*: power deposition spectrum along the radial direction (P_r) evaluated for different axial wave numbers k_z. a) Center of the discharge z = 0 m; b) boundary of the discharge z = 0.05 m.

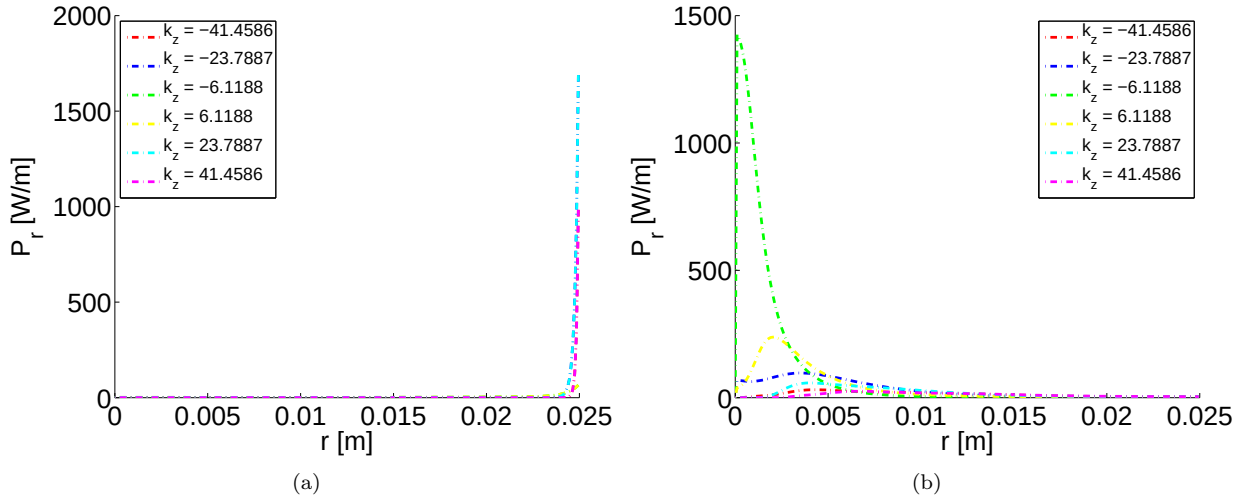

Figure 10. Helmholtz's coil configuration *Case High*: power deposition spectrum along the radial direction (P_r) evaluated for different axial wave numbers k_z. a) Center of the discharge z = 0 m; b) boundary of the discharge z = 0.05 m.

IV. Conclusion

We have analyzed two configurations of actual magneto-static field, namely those generated by Maxwell's, and Helmholtz's coils. For each magnetic field configuration we have studied three cases: i) low-density $n = 10^{17}$ m^{-3} and low-magnetic-field $B_0 = 250$ G; ii) medium-density $n = 10^{18}$ m^{-3} and medium-magnetic-field $B_0 = 500$ G; iii) high-density $n = 10^{19}$ m^{-3} and high-magnetic-field $B_0 = 1000$ G. We have found that the Maxwell coil configuration does not produces significant changes in the deposited power profile in respect to perfectly uniform and axial magneto-static field. While the Helmholtz coil configuration leads to a power deposition profile peaked near the axis of the discharge at the boundary axial section of the source, where the ration between B_{0r} and B_{0z} is approximately 10%. For both magnetic field configurations we have noticed that the power deposition profile peak is higher increasing plasma density and magnetic field strength.

References

[1]Pavarin, D., *et al.*, "Design of 50 W helicon plasma thruster", *31st Int. Electric Propulsion Conf.*, Ann Arbor, MI. 2009.

[2]Chen, F. F., "Helicon plasma sources", *High Density Plasma Sources*, 1995, pp. 1–75.

[3]Chen, F. F., and Arnush, D., "Generalized theory of helicon waves I. Normal modes", *Phys. Plasmas*, Vol. 4, No. 9, 1997, pp. 3411–3421.

[4]Chang Diaz, F. R., "The Vasimir", *Sci. Am.*, Vol. 283, No. 5, November 2000, pp. 90–97.

[5]Pavarin, D., *et al.*, "Helicon Plasma Hydrazine Combined Micro Project Overview and Development Status", *Proceedings of the Space Propulsion Conference*, San Sebastian, Spain, 2010.

[6]Mazari Villanova, L., Papi L., "SAPERE - Space Advanced Project for Excellence in Research and Enterprise", DTA/20-2015.

[7]Arnush, D., and Chen, F. F., "Generalized theory of helicon waves. II. Excitation and absorption", *Physics of Plasmas*, Vol. 5, No. 5, 1998, pp. 1239–1254.

[8]Chen, F. F., and Blackwell, D. D., "Upper limit to Landau damping in helicon discharges", *Physical Review Letters*, Vol. 82, No. 13, 2677, 1999.

[9]Kramer, M., "Propagation and damping of m=+ 1 and m= 1 helicon modes in an inhomogeneous plasma column", *Physics of Plasmas*, Vol. 6, No. 4, 1999, pp. 1052–1058.

[10]Breizman, B. N., and Arefiev, A. V., "Radially localized helicon modes in nonuniform plasma", *Physical Review Letters*, Vol. 84, No. 17, 3863, 2000.

[11]Mouzouris, Y., and Scharer, J. E., "Modeling of profile effects for inductive helicon plasma sources", *IEEE transactions on plasma science*, Vol. 24, No. 1, 1996, pp. 152–160

[12]Chen, G., *et al.*, "Resonant power absorption in helicon plasma sources", *Physics of Plasmas*, Vol. 13, No. 12, 123507, 2006.

[13]Braginskii, O. V., Vasileva, A. N., and Kovalev, A. S., "Helicon plasma in a nonuniform magnetic field", *Plasma Physics Reports*, Vol. 27, No. 8, 2001, pp. 699–707.

[14]Virko, V. F., *et al.*, "Wave phenomena, hot electrons, and enhanced plasma production in a helicon discharge in a converging magnetic field", *Physics of Plasmas*, Vol. 11, No. 8, 2004, pp. 3888–3897.

[15]Guo, X. M., *et al.*, "Helicon experiments and simulations in nonuniform magnetic field configurations", *Physics of Plasmas*, Vol. 6, No. 8, 1999, pp. 3400–3407.

[16]Lafleur, T., Charles, C., and Boswell, R. W., "Characterization of a helicon plasma source in low diverging magnetic fields", *Journal of Physics D: Applied Physics*, Vol. 44, No.5, 055202, 2011.

[17]Lafleur, T., Charles, C., and Boswell, R. W., "Plasma control by modification of helicon wave propagation in low magnetic fields", *Physics of Plasmas*, Vol. 17, No. 7, 073508, 2010.

[18]Chang, L., *et al.*, "Wave modeling in a cylindrical non-uniform helicon discharge", *Physics of Plasmas*, Vol. 19, No. 8, 083511, 2012.

[19]Kinder, R. L., and Kushner, M. J. "Wave propagation and power deposition in magnetically enhanced inductively coupled and helicon plasma sources", *Journal of Vacuum Science & Technology A*, Vol. 19, No. 1, 2001, pp. 76–86.

[20]Bose, D., Govindan, T. R., and Meyyappan, M., "Modeling of a helicon plasma source", *IEEE transactions on plasma science*, Vol. 31, No. 4, 2003, pp. 464–470.

[21]D. Melazzi, *et al.*, "SPIREs: A Finite-Difference Frequency-Domain electromagnetic solver for inhomogeneous plasma cylinders", *Computer Physics Communications*, Vol.183, No. 6, 2012, pp. 1182–1191.

[22]Stix, T. H., "The theory of plasma waves", *The Theory of Plasma Waves*, New York: McGraw-Hill, 1962.

[23]Cardinali, *et al.*, "Ray-tracing WKB analysis of Whistler waves in non-uniform magnetic fields applied to space thrusters", *Plasma Sources Science and Technology*, Vol 23, No. 1, 015013, 2014.

[24]Swanson, D. G., "Plasma waves", 2nd edition, *Elsevier*, 2012.